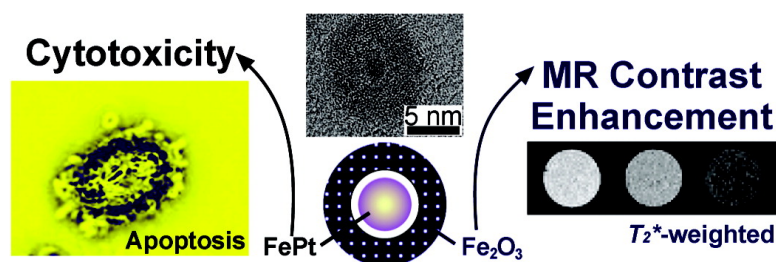Article

Multifunctional Yolk#Shell Nanoparticles: A Potential MRI Contrast and Anticancer Agent

Jinhao Gao, Gaolin Liang, Jerry S. Cheung, Yue Pan, Yi Kuang, Fan Zhao, Bei Zhang, Xixiang Zhang, Ed X. Wu, and Bing Xu

More About This Article

Additional resources and features associated with this article are available within the HTML version:

- Supporting Information
- Access to high resolution figures
- Links to articles and content related to this article
- Copyright permission to reproduce figures and/or text from this article

View the Full Text HTML

Multifunctional Yolk–Shell Nanoparticles: A Potential MRI Contrast and Anticancer Agent

Jinhao Gao,[†] Gaolin Liang,[‡] Jerry S. Cheung,[§] Yue Pan,[†] Yi Kuang,[‡] Fan Zhao,[†] Bei Zhang,[||] Xixiang Zhang,[||] Ed X. Wu,[§] and Bing Xu*,[†,‡]

Department of Chemistry, Bioengineering Program, and Department of Physics, The Hong Kong University of Science and Technology, Clear Water Bay, and Laboratory of Biomedical Imaging and Signal Processing, Department of Electrical and Electronic Engineering, The University of Hong Kong, Pokfulam Road, Hong Kong, China

Received May 25, 2008; E-mail: chbingxu@ust.hk

Abstract: We report a new type of multifunctional nanomaterials, FePt@Fe$_2$O$_3$ yolk–shell nanoparticles, that exhibit high cytotoxicity originated from the FePt yolks and strong MR contrast enhancement resulting from the Fe$_2$O$_3$ shells. Encouraged by the recently observed high cytotoxicity of FePt@CoS$_2$ yolk–shell nanoparticles, we used Fe$_2$O$_3$ to replace CoS$_2$ as the shells to further explore the applications of the yolk–shell nanostructures. The ultralow IC$_{50}$ value (238 ± 9 ng of Pt/mL) of FePt@Fe$_2$O$_3$ yolk–shell nanoparticles likely originates from the fact that the slow oxidation and release of FePt yolks increases the cytotoxicity. Moreover, compared with two commercial magnetic resonance imaging (MRI) contrast agents, MION and Sinerem, the FePt@Fe$_2$O$_3$ yolk–shell nanoparticle showed stronger contrast enhancement according to their apparent transverse relaxivity values ($r_2^* = 3.462$ (μg/mL)$^{-1}$ s^{-1}). The bifunctional FePt@Fe$_2$O$_3$ yolk–shell nanoparticles may serve both as an MRI contrast agent and as a potent anticancer drug. This work indicates that these unique yolk–shell nanoparticles may ultimately lead to new designs of multifunctional nanostructures for nanomedicine.

Introduction

In this paper we describe FePt@Fe$_2$O$_3$ yolk–shell nanoparticles to exhibit both a magnetic resonance imaging (MRI) contrast enhancing effect and a potent cytotoxicity toward HeLa cells. Because of the capability of combining multiple functionalities into a single entity on the nanoscale in an unprecedented way, nanotechnology offers the opportunity to develop a multifunctional nanostructure for multipurpose applications; for example, such nanostructures can not only monitor and detect the cellular changes associated with disease pathogenesis but also treat the disease at the cellular level. Recently, the multidisciplinary developments in the fields of physics, chemistry, and biology have led to the rational design and use of multifunctional nanomaterials for biomedical applications, such as cell imaging, drug delivery, diagnosis, and therapeutics.[1−11] Among the nanostructures being actively explored, magnetic nanomaterials (e.g., Fe$_3$O$_4$ nanoparticles and γ-Fe$_2$O$_3$ nanoparticles) are emerging as a new type of nanomedicine for the

treatment of various diseases (e.g., cancers) because they can serve as MRI contrast agents[12−19] or as magnetic-field-guided

† Department of Chemistry, The Hong Kong University of Science and Technology.
‡ Bioengineering Program, The Hong Kong University of Science and Technology.
§ The University of Hong Kong.
|| Department of Physics, The Hong Kong University of Science and Technology.

(1) Michalet, X.; Pinaud, F. F.; Bentolila, L. A.; Tsay, J. M.; Doose, S.; Li, J. J.; Sundaresan, G.; Wu, A. M.; Gambhir, S. S.; Weiss, S. *Science* **2005**, *307*, 538.
(2) Rosler, A.; Vandermeulen, G. W. M.; Klok, H. A. *Adv. Drug Delivery Rev.* **2001**, *53*, 95.
(3) Weissleder, R. *Science* **2006**, *312*, 1168.
(4) Svenson, S.; Tomalia, D. A. *Adv. Drug Delivery Rev.* **2005**, *57*, 2106.
(5) So, M. K.; Xu, C. J.; Loening, A. M.; Gambhir, S. S.; Rao, J. H. *Nat. Biotechnol.* **2006**, *24*, 339.
(6) Zhang, Y.; So, M. K.; Loening, A. M.; Yao, H. Q.; Gambhir, S. S.; Rao, J. H. *Angew. Chem., Int. Ed.* **2006**, *45*, 4936.
(7) Cai, W. B.; Chen, X. Y. *Small* **2007**, *3*, 1840.
(8) McCarthy, J. R.; Kelly, K. A.; Sun, E. Y.; Weissleder, R. *Nanomedicine* **2007**, *2*, 153.
(9) Chen, J. Y.; Wang, D. L.; Xi, J. F.; Au, L.; Siekkinen, A.; Warsen, A.; Li, Z. Y.; Zhang, H.; Xia, Y. N.; Li, X. D. *Nano Lett.* **2007**, *7*, 1318.
(10) Yang, H.; Xia, Y. N. *Adv. Mater.* **2007**, *19*, 3085.
(11) Alric, C.; Taleb, J.; Le Duc, G.; Mandon, C.; Billotey, C.; Le Meur-Herland, A.; Brochard, T.; Vocanson, F.; Janier, M.; Perriat, P.; Roux, S.; Tillement, O. *J. Am. Chem. Soc.* **2008**, *130*, 5908.
(12) Lewin, M.; Carlesso, N.; Tung, C. H.; Tang, X. W.; Cory, D.; Scadden, D. T.; Weissleder, R. *Nat. Biotechnol.* **2000**, *18*, 410.
(13) Corot, C.; Robert, P.; Idee, J. M.; Port, M. *Adv. Drug Delivery Rev.* **2006**, *58*, 1471.
(14) Lee, J. H.; Huh, Y. M.; Jun, Y.; Seo, J.; Jang, J.; Song, H. T.; Kim, S.; Cho, E. J.; Yoon, H. G.; Suh, J. S.; Cheon, J. *Nat. Med.* **2007**, *13*, 95.
(15) Na, H. B.; Lee, J. H.; An, K. J.; Park, Y. I.; Park, M.; Lee, I. S.; Nam, D. H.; Kim, S. T.; Kim, S. H.; Kim, S. W.; Lim, K. H.; Kim, K. S.; Kim, S. O.; Hyeon, T. *Angew. Chem., Int. Ed.* **2007**, *46*, 5397.
(16) Huh, Y. M.; Jun, Y. W.; Song, H. T.; Kim, S.; Choi, J. S.; Lee, J. H.; Yoon, S.; Kim, K. S.; Shin, J. S.; Suh, J. S.; Cheon, J. *J. Am. Chem. Soc.* **2005**, *127*, 12387.
(17) Harisinghani, M. G.; Barentsz, J.; Hahn, P. F.; Deserno, W. M.; Tabatabaei, S.; van de Kaa, C. H.; de la Rosette, J.; Weissleder, R. *N. Engl. J. Med.* **2003**, *348*, 2491.
(18) Seo, W. S.; Lee, J. H.; Sun, X. M.; Suzuki, Y.; Mann, D.; Liu, Z.; Terashima, M.; Yang, P. C.; McConnell, M. V.; Nishimura, D. G.; Dai, H. J. *Nat. Mater.* **2006**, *5*, 971.

drug delivery vehicles.[20−22] The unique properties and exciting applications of magnetic nanomaterials have inspired the fabrication of multifunctional nanostructures based on magnetic nanoparticles, such as FePt−CdX (X = S, Se) heterodimer (or core−shell) nanoparticles,[23,24] Fe_3O_4−Ag or Fe_3O_4−CdSe heterodimer nanoparticles,[25,26] and Au−Fe_3O_4 dumbbell-like bifunctional nanoparticles.[27] Recently, on the basis of the yolk−shell nanostructures reported by Alivisatos and co-workers, we developed FePt@CoS_2 yolk−shell nanoparticles that could serve as an anticancer agent because of their ultrahigh cytotoxicity.[28] The porous shells formed through the Kirkendall effect[29−32] ensure the slow diffusion of platinum ions out of the shells to yield exceptionally high cytotoxicity. The slow dissolution of the uncoated FePt yolks dramatically increases the cytotoxicity of these yolk−shell nanoparticles, which represent a new type of controlled drug delivery system.[33] This finding encouraged us to further study the potential applications of this type of nanostructures on the basis of the surface chemistry of the shell and the composition of the yolk.

Herein, we designed and synthesized FePt@Fe_2O_3 yolk−shell nanoparticles through the Kirkendall effect with FePt nanoparticles[34] serving as the seeds. Because of the cytotoxicity originating from the FePt yolk and MRI effects due to the Fe_2O_3 shell, these FePt@Fe_2O_3 yolk−shell nanoparticles exhibit dual functions, which may lead to a new strategy to combine diagnostic and therapeutic agents. Compared to the conventional treatments of magnetic nanoparticles for drug delivery, such as polymer coatings, which may require complicated processes and result in modest efficiency,[35,36] the direct encapsulation of the precursor of the drugs or the therapeutic agents by the growth of an iron oxide shell could dramatically simplify the production process. Moreover, the strategy described here may lead to a new type of drugs that kill pathogenic cells by slow release of active agents from the yolk−shell magnetic nanoparticles.

Results and Discussion

Fabrication and Characterization of the Multifunctional Yolk−Shell Nanoparticles. Recently, several groups have synthesized iron oxide hollow nanoparticles based on the oxidation of iron nanoparticles by the Kirkendall effect on the

nanoscale,[37−39] which encouraged us to use iron oxide as the shell for yolk−shell nanostructures.[29] Using FePt nanoparticles (about 3 nm in diameter) as the seeds, we directly injected the solution of $Fe(CO)_5$ into the refluxing solution of 1-octadecene containing oleylamine and FePt nanoparticles to form FePt@Fe core−shell nanoparticles as the intermediate (Figure S1, Supporting Information). These as-prepared FePt@Fe core−shell nanoparticles in 1-octadecene were exposed to the ambient atmosphere and heated to 180 °C in the presence of O_2 flowing with a rate of 2 m^3/h. At the end of the 2 h oxidization, FePt@Fe_2O_3 yolk−shell nanoparticles were obtained by centrifugation. As shown in the transmission electron microscopy (TEM) image (Figure 1A), the FePt@Fe_2O_3 yolk−shell nanoparticles have a structure similar to that of other yolk−shell nanoparticles (e.g., FePt@CoS_2[28] or Pt@CoO[29] yolk−shell nanoparticles) due to the Kirkendall effect occurring on the shell of the FePt@Fe core−shell intermediates. The high-resolution TEM (HRTEM) image of FePt@Fe_2O_3 yolk−shell nanoparticles (Figure 1B) indicates that both the FePt yolk and the Fe_2O_3 shell are crystalline.

To investigate the stability of FePt cores in the organic solvent during oxidation, we carried out the oxidation experiment just using the as-prepared FePt nanoparticles under conditions similar to those used for oxidizing FePt@Fe nanoparticles. The TEM images and selected area electron diffraction pattern (EDP) analysis (Figure S2, Supporting Information) indicate that the FePt nanoparticles still maintain a highly crystalline structure (fcc phase) without a significant size change after oxidation. Magnetism analysis (Figure S2, Supporting Information) shows that the FePt nanoparticles retain superparamagnetic behavior with little change in the blocking temperature (∼15 K) after being treated under the oxidative condition. These results confirm that the as-prepared FePt nanoparticles are stable enough in the organic solvent under the oxidization conditions and can serve as the seeds for making the yolk−shell nanoparticles. Energy-dispersive X-ray spectroscopy (EDS) analysis (Figure S3, Supporting Information) indicates that the core of FePt@Fe_2O_3 yolk−shell nanoparticles mainly consists of Fe and Pt and the shell only consists of Fe, suggesting that the FePt cores remain unchanged after the oxidization process. X-ray fluorescence (XRF) spectroscopy analysis indicates that the molar ratio of FePt to Fe_2O_3 is 1:41, corresponding to ∼28.7 ng of Pt/μg of FePt@Fe_2O_3 yolk−shell nanoparticles (Figure S4, Supporting Information).

To investigate the bifunctional FePt@Fe_2O_3 yolk−shell nanoparticles in detail, we further made three other types of relevant nanostructures, Pt@Fe_2O_3 yolk−shell nanoparticles, FePt@Fe_3O_4 core−shell nanoparticles, and γ-Fe_2O_3 hollow nanoparticles, as the control samples. The different yolk compositions (e.g., Pt yolk versus FePt yolk) and the morphologies of the nanostructures (e.g., core−shell versus yolk−shell) would certainly dictate the properties and functions of these nanomaterials. By utilizing Pt nanoparticles as seeds, a method

(19) Xie, J.; Chen, K.; Lee, H. Y.; Xu, C. J.; Hsu, A. R.; Peng, S.; Chen, X. Y.; Sun, S. H. *J. Am. Chem. Soc.* **2008**, *130*, 7542.
(20) Giri, S.; Trewyn, B. G.; Stellmaker, M. P.; Lin, V. S. Y. *Angew. Chem., Int. Ed.* **2005**, *44*, 5038.
(21) Son, S. J.; Reichel, J.; He, B.; Schuchman, M.; Lee, S. B. *J. Am. Chem. Soc.* **2005**, *127*, 7316.
(22) Dobson, J. *Nanomedicine* **2006**, *1*, 31.
(23) Gao, J. H.; Zhang, B.; Gao, Y.; Pan, Y.; Zhang, X. X.; Xu, B. *J. Am. Chem. Soc.* **2007**, *129*, 11928.
(24) Gu, H. W.; Zheng, R. K.; Zhang, X. X.; Xu, B. *J. Am. Chem. Soc.* **2004**, *126*, 5664.
(25) Gu, H. W.; Yang, Z. M.; Gao, J. H.; Chang, C. K.; Xu, B. *J. Am. Chem. Soc.* **2005**, *127*, 34.
(26) Gao, J. H.; Zhang, W.; Huang, P. B.; Zhang, B.; Zhang, X. X.; Xu, B. *J. Am. Chem. Soc.* **2008**, *130*, 3710.
(27) Yu, H.; Chen, M.; Rice, P. M.; Wang, S. X.; White, R. L.; Sun, S. H. *Nano Lett.* **2005**, *5*, 379.
(28) Gao, J. H.; Liang, G. L.; Zhang, B.; Kuang, Y.; Zhang, X. X.; Xu, B. *J. Am. Chem. Soc.* **2007**, *129*, 1428.
(29) Yin, Y. D.; Rioux, R. M.; Erdonmez, C. K.; Hughes, S.; Somorjai, G. A.; Alivisatos, A. P. *Science* **2004**, *304*, 711.
(30) Gao, J. H.; Zhang, B.; Zhang, X. X.; Xu, B. *Angew. Chem., Int. Ed.* **2006**, *45*, 1220.
(31) Fan, H. J.; Gösele, U.; Zacharias, M. *Small* **2007**, *3*, 1660.
(32) Kim, S. H.; Yin, Y. D.; Alivisatos, A. P.; Somorjai, G. A.; Yates, J. T. *J. Am. Chem. Soc.* **2007**, *129*, 9510.
(33) Tabata, Y.; Ikada, Y. *Adv. Drug Delivery Rev.* **1998**, *31*, 287.

(34) Sun, S. H.; Murray, C. B.; Weller, D.; Folks, L.; Moser, A. *Science* **2000**, *287*, 1989.
(35) Neuberger, T.; Schopf, B.; Hofmann, H.; Hofmann, M.; von Rechenberg, B. *J. Magn. Magn. Mater.* **2005**, *293*, 483.
(36) Gupta, A. K.; Gupta, M. *Biomaterials* **2005**, *26*, 3995.
(37) Peng, S.; Wang, C.; Xie, J.; Sun, S. H. *J. Am. Chem. Soc.* **2006**, *128*, 10676.
(38) Peng, S.; Sun, S. H. *Angew. Chem., Int. Ed.* **2007**, *46*, 4155.
(39) Cabot, A.; Puntes, V. F.; Shevchenko, E.; Yin, Y.; Balcells, L.; Marcus, M. A.; Hughes, S. M.; Alivisatos, A. P. *J. Am. Chem. Soc.* **2007**, *129*, 10358.
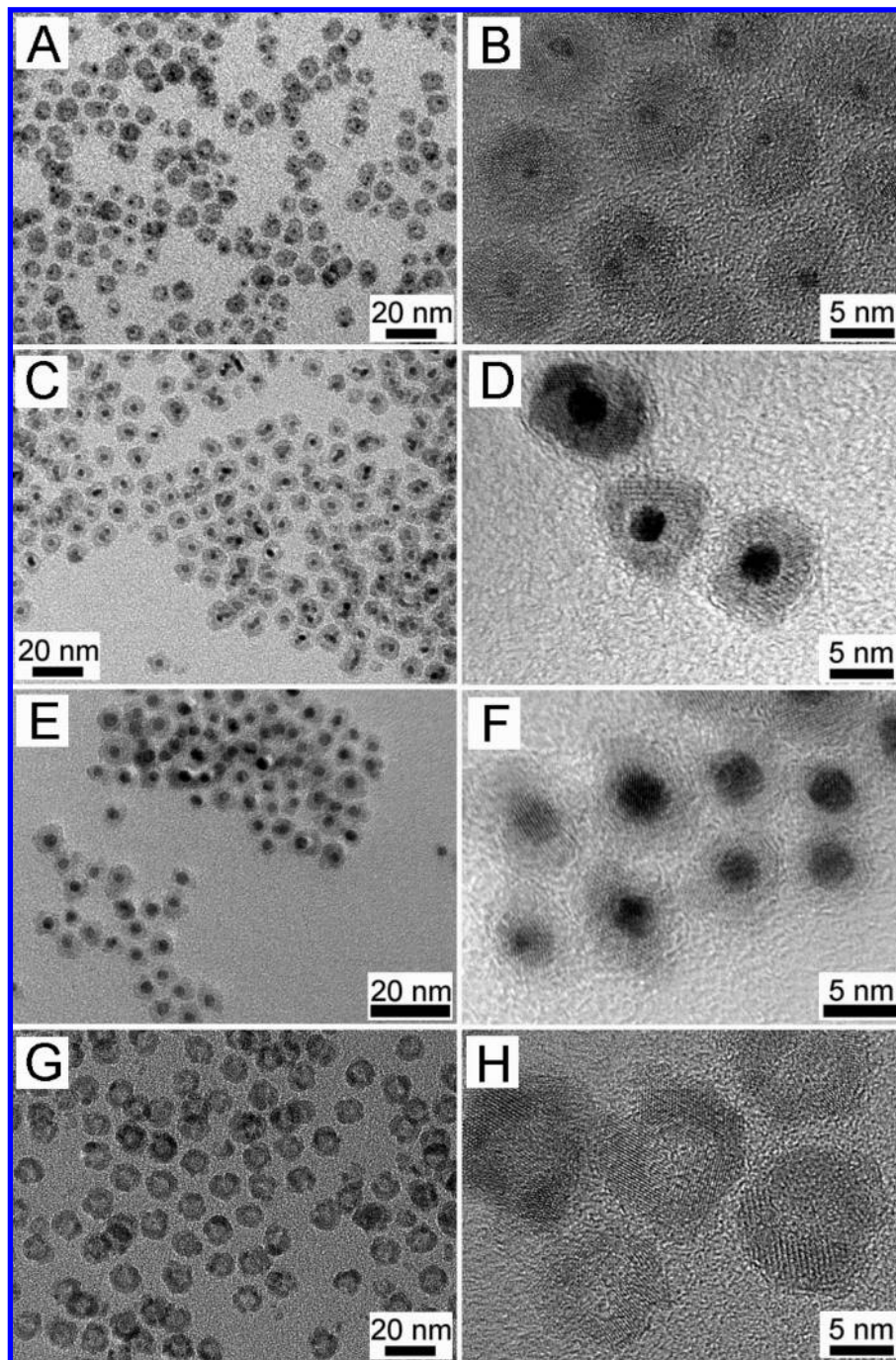
Figure 1. TEM (A, C, E, and G) and HRTEM (B, D, F, and H) images of FePt@Fe$_2$O$_3$ yolk−shell nanoparticles (A, B), Pt@Fe$_2$O$_3$ yolk−shell nanoparticles (C, D), and FePt@Fe$_3$O$_4$ core−shell nanoparticles (E, F) obtained by the seed-growth method and γ-Fe$_2$O$_3$ hollow nanoparticles (G, H) synthesized via the Kirkendall effect.

similar to the synthesis of FePt@Fe$_2$O$_3$ yolk−shell nanoparticles gives Pt@Fe$_2$O$_3$ yolk−shell nanoparticles (Figure 1C,D). FePt@Fe$_3$O$_4$ core−shell nanoparticles (Figure 1E,F) were synthesized by the coating of FePt cores with Fe$_3$O$_4$ shells through the thermal decomposition of Fe(acac)$_3$.[40] The direct oxidization of the as-prepared iron nanoparticles by O$_2$ can give a product of γ-Fe$_2$O$_3$ hollow nanoparticles (Figure 1G,H). Because of the harsh oxidative condition, instead of Fe$_3$O$_4$

(40) Zeng, H.; Li, J.; Wang, Z. L.; Liu, J. P.; Sun, S. H. *Nano Lett.* **2004**, *4*, 187.
(41) Shevchenko, E. V.; Kortright, J. B.; Talapin, D. V.; Aloni, S.; Alivisatos, A. P. *Adv. Mater.* **2007**, *19*, 4183.
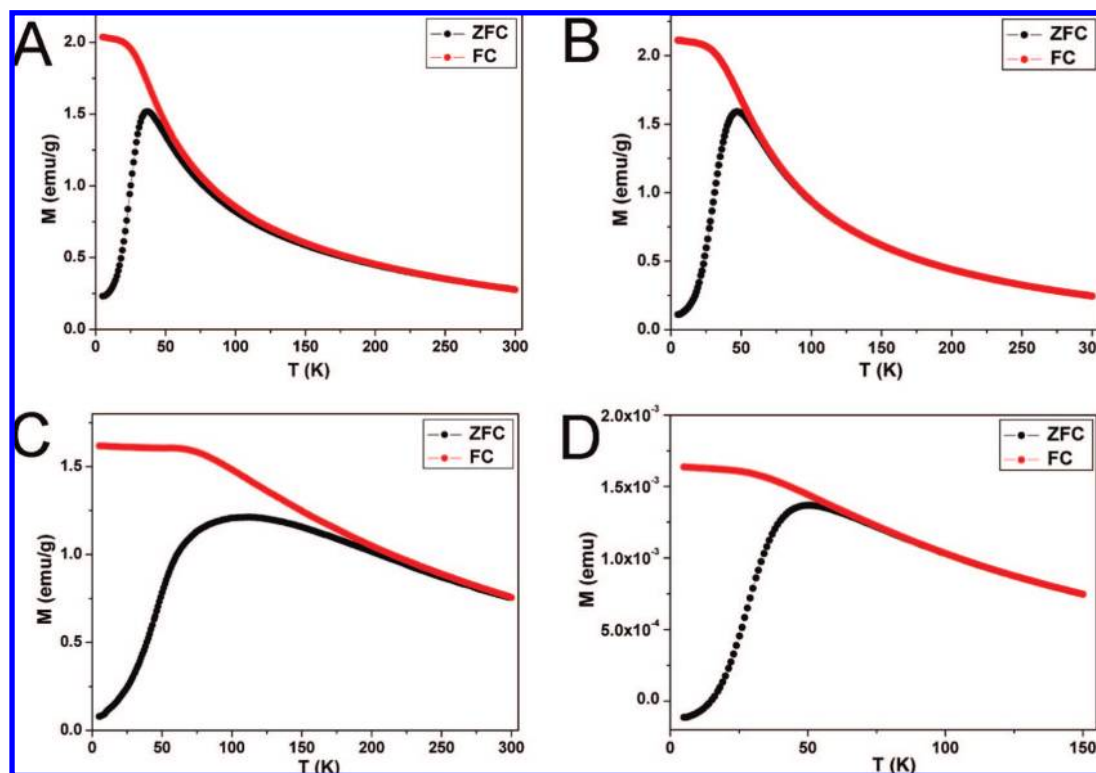
nanoparticles, Fe$_2$O$_3$ nanoparticles become the favorable product. EDP analysis (Figure S5, Supporting Information) indicates that these Fe$_2$O$_3$ hollow nanoparticles are in the γ phase[41] with high crystallinity (Figure 1H), possibly because the oxidation also occurs at a relatively high temperature.

Magnetic Properties. The magnetic measurement, performed immediately after the synthesis of the nanoparticles, reveals the superparamagnetism of these nanostructures. Standard zero-field-cooling (ZFC) and field-cooling (FC) measurements give estimated blocking temperatures of about 36 K for the FePt@Fe$_2$O$_3$ yolk−shell nanoparticles and 46 K for the Pt@Fe$_2$O$_3$ yolk−shell nanoparticles, respectively (Figure 2A,B), suggesting

Figure 2. Temperature dependence of the ZFC/FC magnetization (at a magnetic field of 100 Oe) of (A) FePt@Fe$_2$O$_3$ yolk−shell nanoparticles, (B) Pt@Fe$_2$O$_3$ yolk−shell nanoparticles, (C) FePt@Fe$_3$O$_4$ core−shell nanoparticles, and (D) γ-Fe$_2$O$_3$ hollow nanoparticles in hexane solution.

that they exhibit superparamagnetic behaviors at room temperature. The overall size of the FePt@ Fe$_2$O$_3$ yolk−shell nanoparticles (∼8 nm in diameter) is smaller than that of the Pt@Fe$_2$O$_3$ yolk−shell nanoparticles (∼10 nm in diameter), resulting in a slightly lower blocking temperature of the FePt@Fe$_2$O$_3$ yolk−shell nanoparticles. The well-defined sharp peaks indicate these two kinds of nanoparticle samples having narrow size distributions. SQUID magnetometry (ZFC/FC) measurements of FePt@Fe$_3$O$_4$ core−shell nanoparticles give a blocking temperature of about 110 K with a broad peak (Figure 2C), suggesting that there are strong magnetic dipole−dipole and/or exchange interactions among the particles, in addition to the exchange coupling between FePt cores and Fe$_3$O$_4$ shells within the particles that agrees with the core−shell nanostructures. The blocking temperature of γ-Fe$_2$O$_3$ hollow nanoparticles is about 50 K with a well-defined sharp peak (Figure 2D), due to the large size (∼12 nm in diameter) and the excellent crystallinality of the nanoparticles.

The field-dependent magnetization measurements show that all four of these nanoparticles are superparamagnetic and lack any hysteresis loops at room temperature (Figure 3). The saturated magnetization (M_s) of γ-Fe$_2$O$_3$ hollow nanoparticles is about 50.8 emu/g, the highest value among those four samples, further confirming the high crystallinity of the γ-Fe$_2$O$_3$ hollow nanoparticles. The M_s values are 25.2, 19.5, and 24.8 emu/g for FePt@Fe$_2$O$_3$ yolk−shell, Pt@Fe$_2$O$_3$ yolk−shell, and FePt@Fe$_3$O$_4$ core−shell nanoparticles, respectively.

Investigation of MR Contrast Enhancement. After the simple surface modification of the nanoparticles by 3,4-dihydroxy-L-phenylalanine (L-dopa) molecules, these four types of nanoparticles (FePt@Fe$_2$O$_3$ yolk−shell nanoparticles, Pt@Fe$_2$O$_3$ yolk−shell nanoparticles, FePt@Fe$_3$O$_4$ core−shell nanoparticles, and γ-Fe$_2$O$_3$ hollow nanoparticles) dispersed very well in water
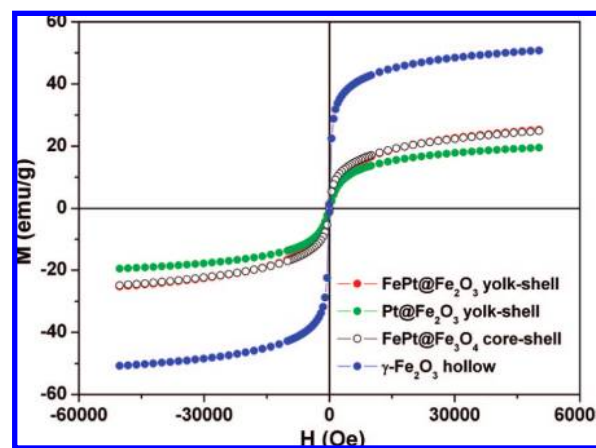

Figure 3. Room-temperature field-dependent magnetization measurements of FePt@Fe$_2$O$_3$ yolk−shell nanoparticles (red circles), Pt@Fe$_2$O$_3$ yolk−shell nanoparticles (green circles), FePt@Fe$_3$O$_4$ core−shell nanoparticles (white circles), and γ-Fe$_2$O$_3$ hollow nanoparticles (blue circles).

(Figure S6, Supporting Information) because L-dopa or its analogues (e.g., dopamine) can serve as stable, hydrophilic surface modifiers for iron oxide nanoparticles.[42] To compare the MR apparent transverse relaxivities (r_2*) of these magnetic nanoparticles, we acquired multiecho gradient echo images (TR (repetition time) = 2 s with TEs (echo times) of 3, 6, 9, 12, 15, 18, 21, 24, 27, 30, 33, 36, 39, 42, 45, and 48 ms and a flip angle of 30°) for each sample with a 7 T MRI scanner with a maximum gradient of 360 mT/m. As shown in Figure 4, γ-Fe$_2$O$_3$ hollow nanoparticles exhibit the strongest MR signal attenuation effect among five types of particles (the above-mentioned four
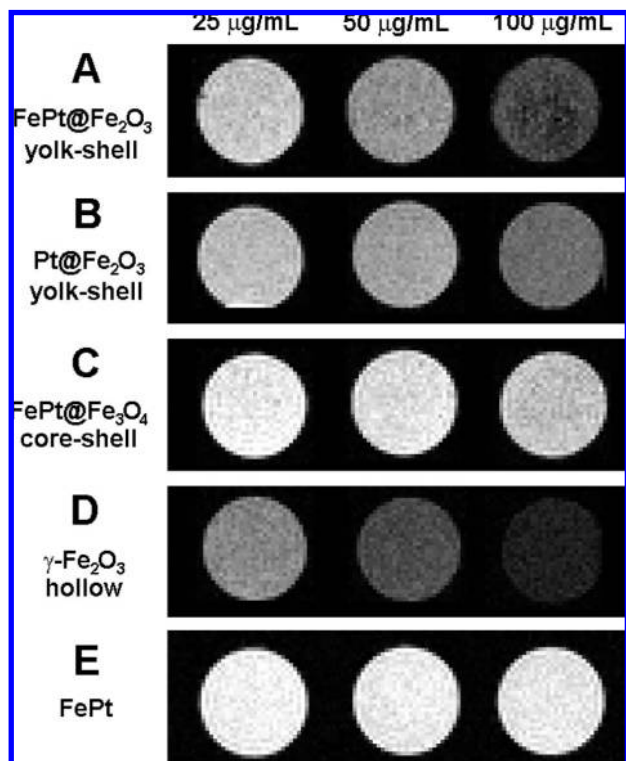
---

(42) Gao, J. H.; Xu, B. Unpublished results.

Figure 4. T_2*-weighted MR images of (A) FePt@Fe$_2$O$_3$ yolk−shell nanoparticles, (B) Pt@Fe$_2$O$_3$ yolk−shell nanoparticles, (C) FePt@Fe$_3$O$_4$ core−shell nanoparticles, (D) γ-Fe$_2$O$_3$ hollow nanoparticles, and (E) FePt nanoparticles from a 7.0 T MRI system at 25, 50, and 100 μg/mL in water (containing 1% agarose gel).

Table 1. Relaxation Rate (R_2*) and Relaxivity (r_2*) Values of the Samples

sample	R_2* at 40 μg/mL (s^{-1})	r_2* [(μg/mL)$^{-1}$s^{-1}]
FePt@Fe$_2$O$_3$ yolk−shell	125.2	3.462
Pt@Fe$_2$O$_3$ yolk−shell	72.1	1.581
FePt@Fe$_3$O$_4$ core−shell	50.0	1.053
γ-Fe$_2$O$_3$ hollow	438.9	10.466
FePt	7.2	0.179
MION	111.1	2.778
Sinerem	98.0	2.450

samples and cysteine-coated FePt nanoparticles, FePt@Cys nanoparticles[28]). FePt@Fe$_2$O$_3$ yolk−shell nanocrystals and Pt@Fe$_2$O$_3$ yolk−shell nanoparticles also showed strong MR relaxation enhancement. However, FePt@Fe$_3$O$_4$ core−shell nanoparticles and FePt@Cys nanoparticles (∼3 nm in diameter) exhibit a very weak MR contrast enhancement effect. The control of magnetic spins by changing the structure of the nanoparticles might be critical for modulating the spin−spin relaxation processes of protons in the water molecules surrounding the nanoparticles,[43] especially for hollow or solid nanoparticles. We used relaxivity values (r_2*) to quantitatively evaluate the MR contrast enhancement for these five samples (Table 1). The r_2* values are 3.462, 1.581, 1.053, 10.466, and 0.179 (μg/mL)$^{-1}$ s^{-1}, respectively, for FePt@Fe$_2$O$_3$ yolk−shell, Pt@Fe$_2$O$_3$ yolk−shell, FePt@Fe$_3$O$_4$ core−shell, γ-Fe$_2$O$_3$ hollow, and FePt@Cys nanoparticles. Compared with two commercial contrast agents, MION (r_2* = 2.778 (μg/mL)$^{-1}$ s^{-1})

and Sinerem (r_2* = 2.450 (μg/mL)$^{-1}$ s^{-1}),[44,45] along with γ-Fe$_2$O$_3$ hollow nanoparticles, FePt@Fe$_2$O$_3$ yolk−shell nanoparticles also show much stronger MR contrast enhancement, suggesting that FePt@Fe$_2$O$_3$ yolk−shell nanoparticles potentially can serve as a novel, efficient MR contrast agent. It is noteworthy that this is the first report of the MRI of hollow magnetic nanoparticles suggesting that hollow magnetic nanoparticles may exhibit advantages in MR relaxation enhancement due to their unique geometry. The interface between the iron oxide hollow nanoparticles and water phase is much larger than that of solid nanoparticles under the same concentrations, which may contribute to the stronger MR contrast enhancement per unit weight.

Cell Assay. We used these water-dispersible nanoparticles to treat HeLa cells for 3 days over the same range of dosages for evaluating their cytotoxicities. According to the 3-(4,5-dimethylthiazol-2-y1)-2,5-diphenyltetrazolium bromide (MTT) assay results (Figure 5), FePt@Fe$_2$O$_3$ yolk−shell nanoparticles have the highest cytotoxicity among these four types of nanoparticles. Likely due to the same possible mechanism of cytotoxicity of FePt@CoS$_2$ yolk−shell nanoparticles,[28] FePt@Fe$_2$O$_3$ yolk−shell nanoparticles showed an ultralow IC$_{50}$ value in terms of Pt (238 ± 9 ng of Pt/mL), which is similar to that of cisplatin (230 ng of Pt/mL).[46] According to the mechanism, the platinum ions, resulting from the oxidization and disruption of the "naked" FePt yolks (Figure S8, Supporting Information), likely bind with DNA double helix structures, interrupt the replication and transcription process, and lead to apoptosis of the HeLa cells. The Pt nanocrystals in Pt@Fe$_2$O$_3$ yolk−shell nanoparticles are stable because of the relative inertness of the Pt yolk. The FePt nanoparticles in FePt@Fe$_3$O$_4$ core−shell nanoparticles are very stable because the biocompatible, compact Fe$_3$O$_4$ shells prevent the oxidative species from reaching the FePt core.[28] Therefore, there are two essential requirements for this kind of nanostructures to serve as an effective drug to kill cancer cells. One is the relatively reactive platinum-containing yolks to ensure redox reaction under proper conditions to form platinum ions; the other is good permeability of the shells or disruption of the shells to allow the metal ions to diffuse out of or be released from the shells. This result suggests that yolk−shell nanoparticles may evolve to become useful and effective drugs for the treatment of cancer.

Conclusion

Compared with the FePt@CoS$_2$ yolk−shell nanoparticles we have reported recently, FePt@Fe$_2$O$_3$ yolk−shell nanoparticles offer several distinct advantages. First, the biocompatibility of Fe$_2$O$_3$ nanoshells ensures the origin of cytotoxicity from the naked FePt yolk and minimizes the possible sources for unwanted side effects caused by the shell. Second, the Fe$_2$O$_3$ nanoshells allow tumor-targeted molecules (e.g., antibodies of specific cancer cells) to be anchored on the shell surface fairly

(43) Koenig, S. H.; Kellar, K. E. *Magn. Reson. Med.* **1995**, *34*, 227.

(44) Wu, E. X.; Wong, K. K.; Andrassy, M.; Tang, H. Y. *Magn. Reson. Med.* **2003**, *49*, 765.
(45) Wu, E. X.; Tang, H. Y.; Jensen, J. H. *NMR Biomed.* **2004**, *17*, 478.
(46) Giovagnini, L.; Ronconi, L.; Aldinucci, D.; Lorenzon, D.; Sitran, S.; Fregona, D. *J. Med. Chem.* **2005**, *48*, 1588.
(47) Xu, C. J.; Xu, K. M.; Gu, H. W.; Zheng, R. K.; Liu, H.; Zhang, X. X.; Guo, Z. H.; Xu, B. *J. Am. Chem. Soc.* **2004**, *126*, 9938.
(48) Fan, X. W.; Lin, L. J.; Dalsin, J. L.; Messersmith, P. B. *J. Am. Chem. Soc.* **2005**, *127*, 15843.
(49) Wang, L.; Yang, Z. M.; Gao, J. H.; Xu, K. M.; Gu, H. W.; Zhang, B.; Zhang, X. X.; Xu, B. *J. Am. Chem. Soc.* **2006**, *128*, 13358.
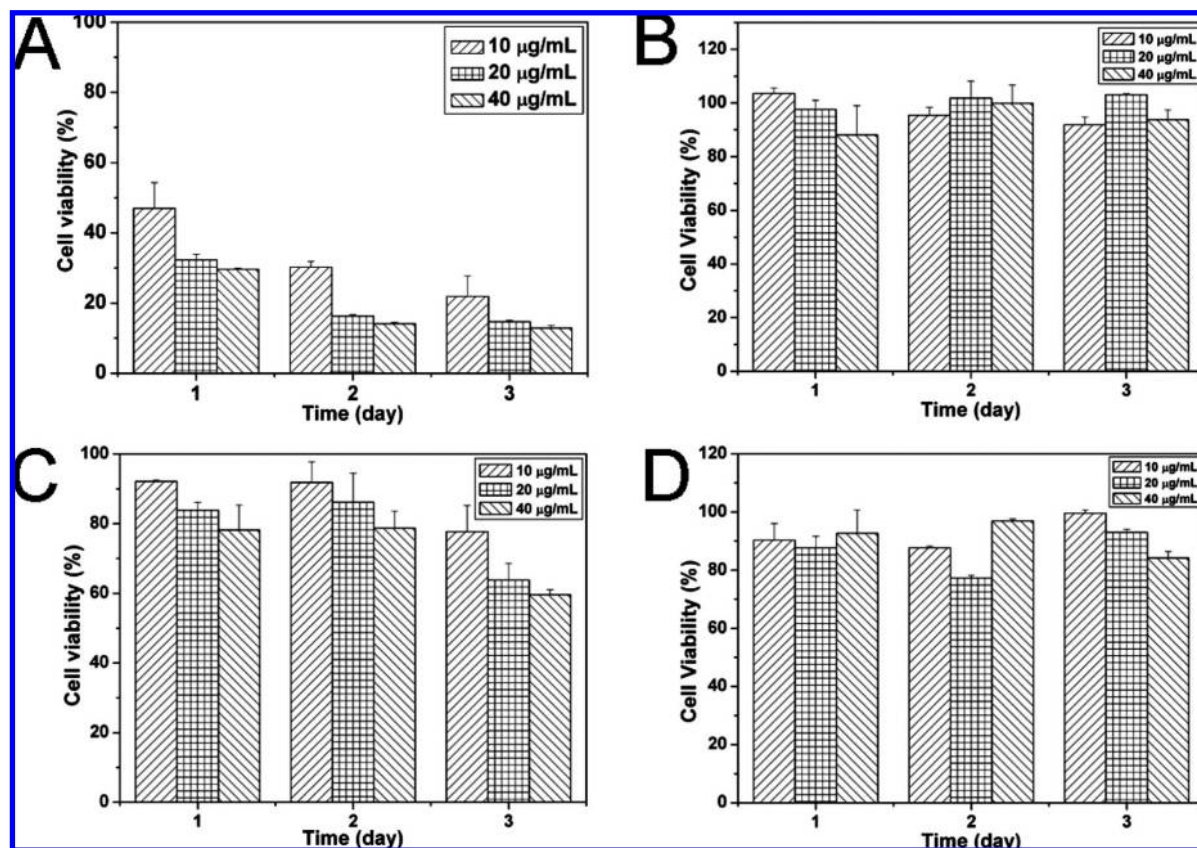
Figure 5. Results of the MTT assay of HeLa cells treated by (A) FePt@Fe$_2$O$_3$ yolk−shell nanocrystals, (B) Pt@Fe$_2$O$_3$ yolk−shell nanoparticles, (C) FePt@Fe$_3$O$_4$ core−shell nanoparticles, and (D) γ-Fe$_2$O$_3$ hollow nanoparticles at 10, 20, and 40 μg/mL for 3 days.

easily by using dopamine and its derivatives as reliable anchors to immobilize functional molecules onto the yolk−shell nanoparticles,[47−51] which would help reduce the side effects. Third, MR relaxation enhancement effects of Fe$_2$O$_3$ nanoshells may provide a direct means for measuring the prognosis during the cancer treatments. Although the long-time stability of Fe$_2$O$_3$ nanoshells in vivo remains to be examined in detail, the bifunctional FePt@Fe$_2$O$_3$ yolk−shell nanoparticles suggest that this type of nanostructures may lead to novel nanomedicines that perform both diagnostic and therapeutic functions. Given the capability of surface functionalization of these multifunctional nanoparticles by disease-specific molecules (e.g., antibodies), one can develop yolk−shell nanoparticles that target a specific tissue or cell type for delivering therapeutic agents to tumors and detecting and monitoring the transforma-

tion of the tumor by noninvasive MR imaging. Moreover, the investigation of such multifunctional nanostructures may lead to the development of other types of multifunctional magnetic nanomaterials as novel therapeutics.

(50) Lee, H.; Lee, B. P.; Messersmith, P. B. *Nature* **2007**, *448*, 338.

(51) Lee, H.; Dellatore, S. M.; Miller, W. M.; Messersmith, P. B. *Science* **2007**, *318*, 426.